Potent antitumor activity of a urokinase-activated engineered anthrax toxin

Shihui Liu*, Hannah Aaronson†, David J. Mitola†, Stephen H. Leppla*‡, and Thomas H. Bugge†‡

*Oral Infection and Immunity Branch and †Oral and Pharyngeal Cancer Branch, National Institute of Dental and Craniofacial Research, National Institutes of Health, Bethesda, MD 20892

Communicated by John B. Robbins, National Institutes of Health, Bethesda, MD, November 8, 2002 (received for review August 12, 2002)

The acquisition of cell-surface urokinase plasminogen activator activity is a hallmark of malignancy. We generated an engineered anthrax toxin that is activated by cell-surface urokinase *in vivo* and displays limited toxicity to normal tissue but broad and potent tumoricidal activity. Native anthrax toxin protective antigen, when administered with a chimeric anthrax toxin lethal factor, *Pseudomonas exotoxin* fusion protein, was extremely toxic to mice, causing rapid and fatal organ damage. Replacing the furin activation sequence in anthrax toxin protective antigen with an artificial peptide sequence efficiently activated by urokinase greatly attenuated toxicity to mice. In addition, the mutation conferred cell-surface urokinase-dependent toxin activation *in vivo*, as determined by using a panel of plasminogen, plasminogen activator, plasminogen activator receptor, and plasminogen activator inhibitor-deficient mice. Surprisingly, toxin activation critically depended on both urokinase plasminogen activator receptor and plasminogen *in vivo*, showing that both proteins are essential cofactors for the generation of cell-surface urokinase. The engineered toxin displayed potent tumor cell cytotoxicity to a spectrum of transplanted tumors of diverse origin and could eradicate established solid tumors. This tumoricidal activity depended strictly on tumor cell-surface plasminogen activation. The data show that a simple change of protease activation specificity converts anthrax toxin from a highly lethal to a potent tumoricidal agent.

The cellular receptor for urokinase plasminogen activator (uPAR) and its cognate protease ligand, urokinase plasminogen activator (uPA), are overexpressed by virtually all human tumors and can be considered a hallmark of malignant conversion (1–3). The intimate association between cell-surface uPA expression and malignant transformation has been documented for tumors as different as carcinoma of the lung, colon, breast, stomach, pancreas, head and neck, skin, uterus, ovaries, and brain, melanoma, hard and soft tissue sarcoma, and monocytic and myelogenous leukemia. uPA and uPAR are expressed at very low levels in normal tissues, but their expression is induced rapidly in response to tissue injury, thereby providing extracellular proteolysis essential for tissue repair and remodeling (2, 4–6). uPA is secreted as a single chain enzyme (pro-uPA) with very low intrinsic activity and is converted to active two-chain uPA by plasmin (7). Two-chain uPA, in turn, is a potent activator of plasminogen (Plg). This property of Plg has been proposed to lead to a powerful feedback loop that results in both plasmin and active two-chain uPA generation. The formation of two-chain uPA and plasmin requires the regulated assembly of pro-uPA and Plg on the cell surface, mediated by the binding of pro-uPA to uPAR and Plg to ubiquitously expressed cell-surface receptors (2). The net result of this feedback loop is the efficient and localized generation of active uPA and plasmin on the cell surface. Although this pivotal role of uPAR in uPA-mediated cell-surface Plg activation is well defined biochemically (2), the function of uPAR in Plg activation *in vivo* remains controversial, because of conflicting genetic and biochemical data (8–11) and the lack of reagents that can detect the state of activation of the minute amounts of uPA that are present in tissues.

Anthrax toxin, a three-part toxin secreted by *Bacillus anthracis*, consists of protective antigen (PrAg, 83 kDa), lethal factor (LF, 90 kDa), and edema factor (90 kDa; refs. 12–14). The three proteins are individually nontoxic. PrAg binds to a ubiquitously expressed cell-surface receptor, tumor endothelium marker 8 (15), and subsequently is cleaved at the sequence, ^{164}RKKR^{167}, by cell-surface furin or furin-like proteases (16, 17). This cleavage is absolutely required for the subsequent steps in toxin action. The C-terminal 63-kDa fragment (PrAg63) remains bound to the receptor and associates to form a heptamer that binds and translocates up to three molecules of LF and edema factor (18) into the cytosol to induce their cytotoxic events. LF residues 1–254 are sufficient to achieve translocation of ''passenger'' polypeptides to the cytosol of the cells in a PrAg-dependent manner. Thus, a fusion of LF residues 1–254 with the ADP-ribosylation domain of *Pseudomonas* exotoxin A [fusion protein 59 (FP59)] kills any cell possessing the anthrax toxin receptor by causing the ADP ribosylation and inhibition of translation elongation factor 2 (19).

The copious expression of uPA and uPAR by human tumors, the causal relation of Plg activation to tumor invasion, and the restricted expression of uPA and uPAR in normal tissues have made cell-surface uPA an attractive target for the treatment of cancer. Most efforts have focused on developing reagents that inhibit the receptor-binding or enzymatic activity of uPA (2, 3). We have taken a different approach to exploit the unique characteristics of the uPA system for therapeutic intervention in cancer by designing cytotoxic agents specifically activated by tumor cell-surface uPA. The absolute requirement for proteolytic cleavage of PrAg on the cell surface for anthrax toxin activation enables the toxin to be engineered to make its activation depend on other proteases besides furin (20). Here, we show that the insertion of an artificial uPA substrate sequence into the furin loop confers cell-surface uPA-dependent activation to the toxin *in vivo*, dramatically restricts the toxicity of anthrax toxin, and endows the engineered toxin with a potent tumor cell cytotoxicity that can eradicate established tumors. We also present a description of an agent that detects the activity of uPA, rather than protein, *in vivo* and use the agent to elucidate the anatomical sites of urokinase activity in the mouse. Moreover, by using mice deficient in components of the plasminogen-activation system, we unequivocally demonstrate that both uPAR and Plg are critical cofactors for the cellular activation of pro-uPA *in vivo*.

Materials and Methods

Mice and Genotype Analysis. The generation of uPA$^{-/-}$ (21), tPA$^{-/-}$ (21), uPA$^{-/-}$/tPA$^{-/-}$ (21), uPAR$^{-/-}$ (8), Plg$^{-/-}$ (22), and PAI-1$^{-/-}$ (23) mice has been described. All mice were

Abbreviations: FP59, fusion protein of LF residues 1–254 and *Pseudomonas* exotoxin A domain III; LF, anthrax toxin lethal factor; PAI-1, plasminogen activator inhibitor-1; PrAg, anthrax toxin-protective antigen; Plg, plasminogen; uPA, urokinase plasminogen activator; uPAR, uPA receptor; TUNEL, terminal deoxynucleotidyltransferase-mediated dUTP nick-end labeling.

‡To whom correspondence should be addressed at: 30 Convent Drive, Bethesda, MD 20892. E-mail: Leppla@nih.gov or thomas.bugge@nih.gov.

backcrossed at least seven times to C57BL/6J (The Jackson Laboratory). The genotypes of the mice were determined by PCR, as described (9, 24). The mice were housed in a pathogen-free facility certified by the Association for Assessment and Accreditation of Laboratory Animal Care International, and the study was carried out in accordance with institutional guidelines.

Determination of the Maximum Tolerated Dose of Recombinant Toxins. PrAg, PrAg-U2, PrAg-U7, and FP59 were prepared as described (25, 26). The maximum tolerated dose was determined by using a dose-escalation protocol aimed at minimizing the number of mice to be used. The mice were anesthetized by isoflurane inhalation and injected i.p. with recombinant toxin in 200 μl of PBS or with PBS alone. The mice were monitored closely for signs of toxicity including weight loss, inactivity, loss of appetite, inability to groom, ruffling of fur, and shortness of breath, and they were euthanized by CO_2 inhalation at the onset of obvious malaise. The maximum tolerated dose was determined as the highest dose in which outward disease or histological tissue damage was not observed in any mice within a 14-day period of observation. The significance of differences between treatment groups was determined by two-tailed χ^2 analysis.

Histological Analysis. Mice were injected with recombinant toxin in PBS or PBS alone. At the onset of malaise or after 24–36 h, the mice were killed by a brief CO_2 inhalation and perfused intracardially with cold PBS, followed by 4% (wt/vol) paraformaldehyde. The organs or tumors were postfixed for 24 h in 4% (wt/vol) paraformaldehyde, embedded in paraffin, sectioned, stained with hematoxylin/eosin, and subjected to microscopic analysis by a pathologist unaware of treatment or animal genotype (two to eight mice per treatment group and genotype). Immunostaining was performed with a Vectastain ABC peroxidase kit (Vector Laboratories), with diaminobenzidine as chromogenic substrate, by using rat anti-mouse CD45R/B220 antibodies (PharMingen) to detect B lymphocytes, rabbit anti-human T cell antibodies (DAKO) to detect T cells, rat anti-mouse CD31 (PECAM-1; PharMingen) to detect endothelial cells, and rat anti-mouse F4/80 (Caltag, South San Francisco, CA) to detect macrophages. Apoptotic cells were visualized by terminal deoxynucleotidyltransferase-mediated dUTP nick-end labeling (TUNEL) by using an Apotag kit (Serologicals, Norcross, GA), and proliferating cells were visualized by injecting mice with BrdUrd 2 h before killing and the staining of sections with BrdUrd antibodies (DAKO).

Tumor Transplantation and Toxin Treatment Assays. Murine B16-BL6 melanoma cells (27) and Lewis lung carcinoma cells (kindly provided by Judah Folkman, Harvard Medical School, Boston) were grown in DMEM with 0.45% glucose/10% FCS/2 mM glutamine/50 μg/ml gentamicin. Murine T241 fibrosarcoma cells (28) (kindly provided by Todd Hembrough, Entremed, Rockville, MD) were grown in DMEM supplemented with 1 mM sodium pyruvate, nonessential amino acid mix, MEM Eagle essential amino acid mix, MEM essential vitamin mix, L-glutamine, penicillin/streptomycin/fungizone mix (all from Bio-Whittaker), and 10% (vol/vol) FCS. The tumor cells were detached by trypsinization and washed once in DMEM containing 10% (vol/vol) FCS and once with cold, serum-free medium. The dorsal skin of mice was shaved 1 day before injection, and isoflurane inhalation-anesthetized mice were injected intradermally between the shoulder blades with 0.3×10^6 T241, 0.5×10^6 B16-BL6, or 0.5×10^6 Lewis lung carcinoma cells in 100 μl of serum-free DMEM. Fifteen micrograms of PrAg-U2 combined with 5 μg of FP59 in 100 μl of PBS or 100 μl of PBS alone was injected intradermally adjacent to the tumor nodule when the tumors had reached a size ranging from ≈0.05% to 0.5% of total body mass (day 0), followed by a second injection of recombinant toxin or PBS at day 3. The longest and shortest tumor diameter was determined daily by calipation by an investigator unaware of treatment group or mouse genotype, and the tumor weight was calculated by using the formula: milligrams = [length in mm × (width in mm)^2]/2 (29). The experiment was terminated when one or more mice in a treatment group presented frank tumor ulceration, to comply with Institutional guidelines. The significance of differences in tumor size was determined by two-tailed Student's t test, and that of differences in frequencies of complete tumor regression was determined by two-tailed χ^2 analysis.

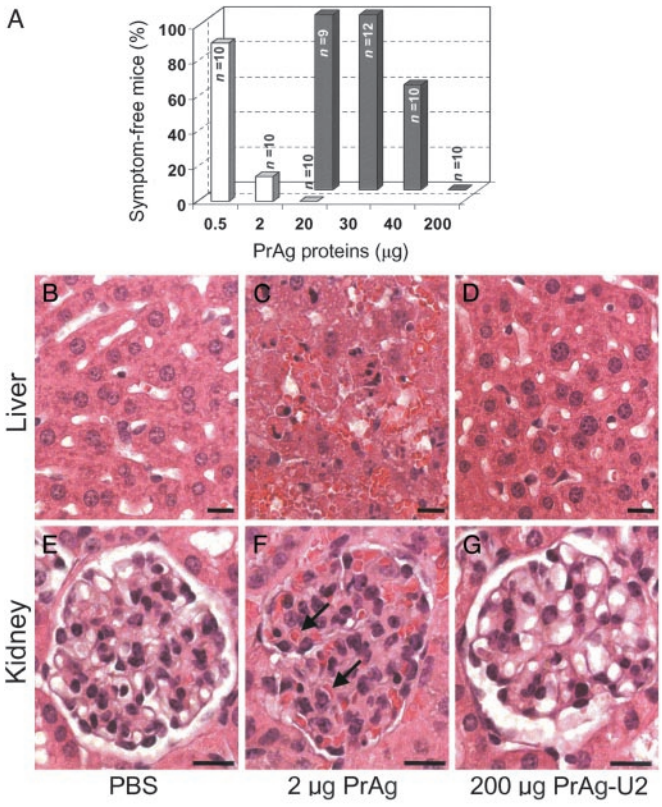

Fig. 1. Furin-to-uPA activation switch attenuates anthrax toxin. (*A*) Mice were challenged by i.p. injection of varying amounts of PrAg (white bars) or PrAg-U2 (black bars) in combination with 10 μg of FP59 and monitored for outward and histological signs of intoxication. (*B–G*) Examples of attenuated organ toxicity of PrAg-U2. Microscopic appearance of liver (*B–D*) and kidneys (*E–G*) of mice 24 h after treatment with PBS (*B* and *E*), 6 h after treatment with 2 μg of PrAg with 10 μg of FP59 (*C* and *F*), or 24 h after treatment with 200 μg of PrAg-U2 with 10 μg of FP59 (*D* and *G*). PrAg treatment causes extensive hepatocellular liquefaction necrosis and angiectasis (*C*) and severe glomerular thickening with associated cellular entrapment (examples indicated with black arrows, *F*), whereas no pathological changes are observed in the liver and kidneys of mice treated with a 100-fold-higher concentration of PrAg-U2 (*D* and *G*). (Bars = 10 μm.)

Results

Furin-to-Urokinase Activation Switch Attenuates and Restricts the Toxicity of Anthrax Toxin. PrAg-U2 is a modified anthrax toxin PrAg in which the furin cleavage site ^{164}RKKR^{167} is replaced by an artificial uPA substrate sequence, SGRSA. PrAg-U2, when administered with FP59, displays uPA-dependent cytotoxicity to cultured cells expressing uPAR (26). We first determined the toxicity of the engineered toxin by challenging mice with 10 μg of FP59 combined with increasing amounts of PrAg-U2, native PrAg, or PrAg-U7 (an uncleavable PrAg variant; ref. 26) or with FP59 and PrAg alone (Fig. 1). The injected mice were observed carefully for outward signs of cytotoxicity, such as inactivity, loss

of appetite, inability to groom, ruffling of fur, and shortness of breath (Fig. 1*A*) and, in independent experiments, by a detailed microscopic examination of tissues (Fig. 1 *B–G*). PrAg or FP59, when administered alone, or PrAg-U7 combined with FP59 were nontoxic to mice even in very large doses (200 μg), confirming that proteolytic cleavage of PrAg in the furin loop is essential to induce cytotoxicity of FP59 *in vivo* (data not shown). In contrast, native PrAg was extremely toxic when combined with FP59, and mice challenged with just 2 μg of PrAg in combination with FP59 became terminally ill 6–24 h after toxin administration (Fig. 1*A*). Histological examination of toxin-treated mice at the onset of symptoms of malaise demonstrated widespread organ damage that was grossly incompatible with life, including hepatic liquefaction necrosis and angiectasis, severe glomerular thickening, pulmonary leukocytosis, adrenal necrosis, bone marrow depletion, and depletion of the splenic red pulp, white pulp, and marginal zone (Fig. 1 *C* and *F*; data not shown). In contrast, PrAg-U2, when combined with FP59, displayed highly attenuated toxicity to mice (Fig. 1*A*). Mice challenged with up to 30 μg of PrAg-U2 with 10 μg of FP59 displayed no outward or histological signs of toxicity (Fig. 1*A*). Histological analysis confirmed that the furin loop mutation completely abolished toxicity to major organ systems, including liver, kidneys, and lungs, even when the mice were challenged with 200 μg of the engineered toxin (Fig. 1 *D* and *G*).

PrAg-U2 Is Activated by Cell-Surface uPA *in Vivo*. We next determined the role of cell-surface uPA in PrAg-U2 activation by challenging a series of inbred mouse strains with complete deficiencies in uPA (21), uPAR (8), Plg (22), and PAI-1 (23) with PrAg and PrAg-U2 with FP59 (Fig. 2). Toxicity began to be observed in WT mice when challenged with 40 μg of PrAg-U2 with FP59 (Fig. 1*A*), and all WT mice became terminally ill when challenged with 200 μg of PrAg-U2 with FP59, with cytotoxicity observed in T cell areas of the spleen and lymph nodes, bone marrow, adrenal cortex, and osteoblasts (Fig. 2 *C–G*; data not shown). The sensitivity of all of the gene-deficient mouse strains to native PrAg in combination with FP59 was similar to WT mice (data not shown). In contrast, uPA$^{-/-}$ mice remained completely healthy, even when challenged with 200 μg of PrAg-U2 with FP59 (Fig. 2*A*). Interestingly, uPAR$^{-/-}$ and Plg$^{-/-}$ mice also were insensitive to 200 μg of PrAg-U2 with FP59 (Fig. 2*A*), demonstrating that both uPAR and Plg are essential cofactors in the generation of uPA activity *in vivo*. Microscopic examination of tissues from uPA$^{-/-}$, uPAR$^{-/-}$, and Plg$^{-/-}$ mice challenged with 200 μg of PrAg-U2 with FP59 failed to demonstrate any signs of cytotoxicity to T cell areas of the spleen and lymph nodes, bone marrow, adrenal cortex, and osteogenic tissues (Fig. 2 *H–J*; and data not shown), providing further evidence that PrAg-U2 is activated by cell-surface uPA and demonstrating that these anatomical locations are principal sites of cell-surface uPA activity *in vivo*. Conversely, PAI-1$^{-/-}$ mice were hypersensitive to PrAg-U2 combined with FP59, with a maximum tolerated dose of about 6 μg (Fig. 2*B*). Microscopic analysis of tissues from PAI-1$^{-/-}$ mice treated with just 20 μg of PrAg-U2 with FP59 demonstrated bone marrow, T cell, osteoblast, and adrenal cytotoxicity, similar to WT mice treated with much higher concentrations of the engineered toxin (data not shown). All PrAg-U2-treated PAI-1$^{-/-}$ mice also presented profound edema of the small intestine frequently associated with hemorrhaging into the intestinal lumen (data not shown). This condition was never observed in WT mice, even when treated with a 10-fold-higher concentration of the engineered toxin. Taken together, these experiments unequivocally demonstrate that uPA, the binding of uPA to uPAR, and the activation of pro-uPA by plasmin are critical events in the activation of PrAg-U2 *in vivo*.

Although cell-surface uPA was the principal activator of PrAg-U2 *in vivo*, some toxin activation clearly could take place

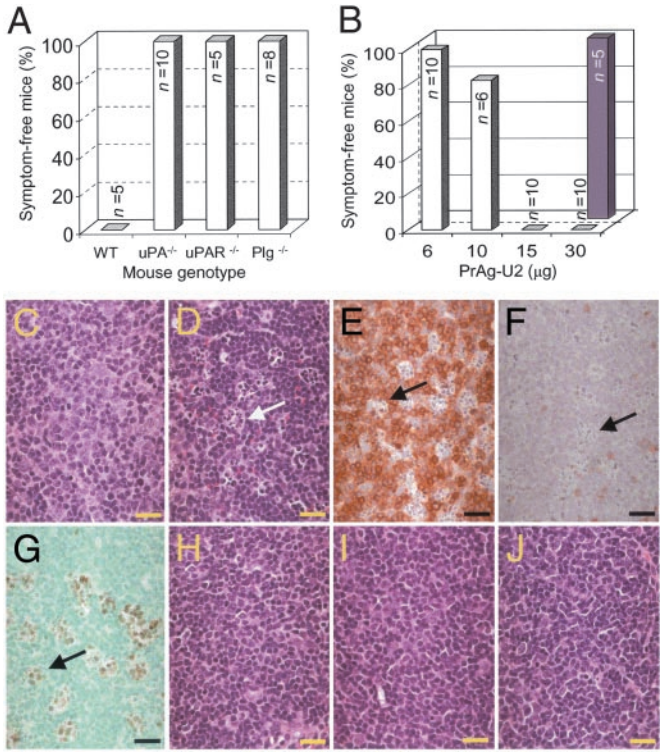

Fig. 2. Furin-to-uPA activation switch confers cell-surface uPA-dependent activation to anthrax toxin *in vivo*. (*A*) Plg-, uPA-, and uPAR-deficient mice are hyper-resistant to uPA-activated anthrax toxin. WT mice and mice deficient in uPA, uPAR, and Plg were challenged with 200 μg of PrAg-U2 with 10 μg of FP59 and were monitored for disease. All WT mice became terminally ill within 24 h of toxin administration, whereas no outward or histological signs of toxicity were detected in uPA-, uPAR-, and Plg-deficient mice ($P < 0.01$). (*B*) PAI-1-deficient mice are hypersensitive to PrAg-U2. PAI-1$^{-/-}$ (white bars) or WT control (black bars) mice were challenged with varying concentrations of PrAg-U2 with 10 μg of FP59 and monitored for disease. All PAI-1$^{-/-}$ mice treated with 15–30 μg of PrAg-U2 became terminally ill within 24 h of toxin administration, whereas no outward or histological signs of toxicity were detected in WT mice challenged with 30 μg of PrAg-U2 ($P < 0.001$). (*C–J*) Cell-surface uPA-dependent T cell toxicity of PrAg-U2: histological appearance of T cell regions of the spleen of WT (*C–G*), uPA$^{-/-}$ (*H*), uPAR$^{-/-}$ (*I*), and Plg$^{-/-}$ (*J*) mice 24 h after i.p. injection of PBS (*C*) or 200 μg of PrAg-U2 with 10 μg of FP59 (*D–J*). Scattered clusters (examples indicated with arrows) of degenerating lymphocytes in WT mice (*D*), absent in PBS-treated WT mice (*C*), are identified as subpopulations of T cells by immunostaining with T cell (*E*) and B cell (*F*) antibodies undergoing apoptosis as visualized by TUNEL staining (*G*). (*H–J*) Absence of T cell pathology in the spleens of uPA$^{-/-}$ (*H*), uPAR$^{-/-}$ (*I*), and Plg$^{-/-}$ (*J*) mice. (*C*, *D*, and *H–J*) Hematoxylin/eosin staining. (Bars = 10 μm.)

in the absence of uPA. Thus, when challenged by repeated injections of PrAg-U2 with FP59, most uPA$^{-/-}$ mice did become ill, suggesting that PrAg-U2 administration sensitizes mice to immediate rechallenge with the engineered toxin (data not shown). We were unable to determine the exact physiological basis of this phenomenon. Possibly, the administration of a high dose of PrAg-U2 with FP59 causes some undetected tissue damage by uPA-independent activation of the toxin, leading to the transiently increased expression of a hypothetical PrAg-U2-activating protease and sensitization of the mice to immediate rechallenge with toxin. This hypothetical protease seemed to be different from tPA, as mice with a combined deficiency in uPA and tPA also were sensitive to repeated daily challenges by PrAg-U2 with FP59 (data not shown).

PrAg-U2 Has Potent and Broad Tumoricidal Activity and Can Eradicate Established Tumors. We evaluated the potential of PrAg-U2 with FP59 for the treatment of cancer by testing the therapeutic

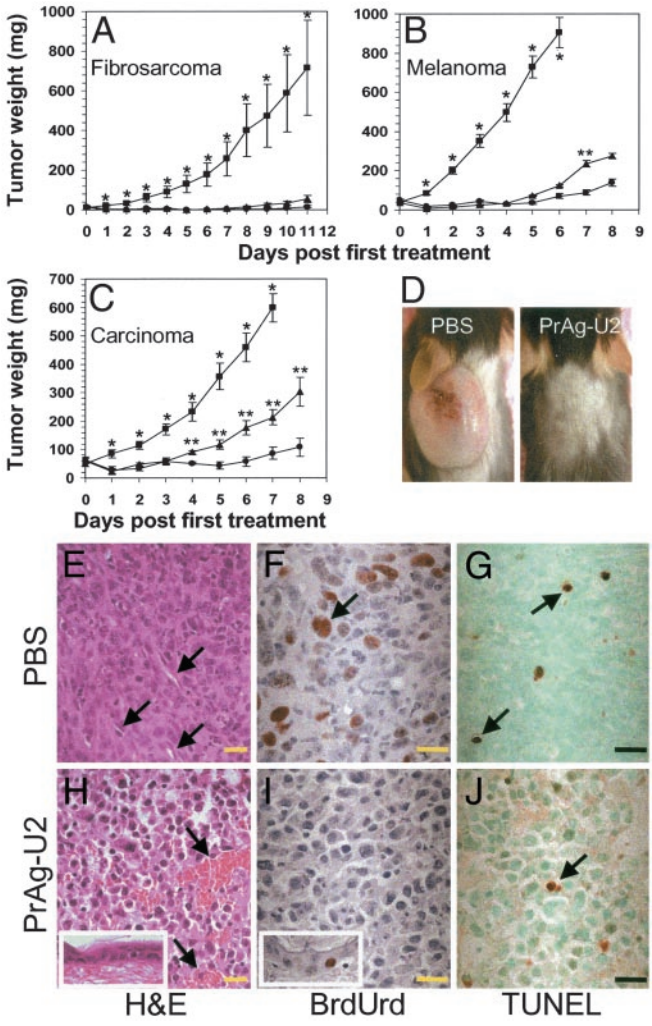

Fig. 3. Potent tumoricidal activity of PrAg-U2. (*A–C*) Broad spectrum PrAg-U2 tumor cytotoxicity. T241 fibrosarcoma-bearing (*A*), B16-BL6 melanoma-bearing (*B*), and Lewis lung carcinoma-bearing (*C*) mice were treated with PBS on day 0 and day 3 (■), 15 μg of PrAg-U2 with 5 μg of FP59 on day 0 and PBS on day 3 (▲), or PrAg-U2 with FP59 on both day 0 and day 3 (●). (*D*) Representative examples of the appearance of T241 fibrosarcoma-bearing mice 14 days after the treatment with PBS (*Left*) or PrAg-U2 (*Right*). Complete tumor regression was observed in six of nine fibrosarcoma-bearing mice treated by a single administration of PrAg-U2 with FP59 ($P < 0.01$), in seven of eight T241 fibrosarcoma-bearing mice treated with two administrations of toxin ($P < 0.001$), and in one of six B16-BL6-bearing mice treated by two administrations of the toxin ($P > 0.05$). The weight of intradermal tumor nodules is expressed as mean tumor weight ± the SEM. *, Significance ($P < 0.05$) of PBS treatment vs. single treatment with PrAg-U2; **, significance of the single treatment with PrAg-U2 at day 0 vs. treatment with PrAg-U2 on both day 0 and day 3. (*E–J*) Selective tumor cell cytotoxicity and tumor endothelial cell damage induced by PrAg-U2. Microscopic appearance of Lewis lung carcinoma 24 h after the treatment of mice with PBS (*E–G*) or 15 μg of PrAg-U2 with 5 μg of FP59 (*H–J*). Hematoxylin/eosin staining (*E* and *H*) reveals extensive tumor cell toxicity and angiectasis with hemorrhage in PrAg-U2-treated (*H*) but not mock-treated (*E*) mice. Examples of vessels are indicated with arrows. (*H Inset*) Normal histological appearance of the epidermis overlying the tumors of toxin-treated mice. BrdUrd incorporation (*F* and *I*) demonstrates complete cessation of DNA synthesis in toxin-treated tumor cells (*I*) but continued proliferation of basal keratinocytes in the epidermis adjacent to the tumor (*I Inset*). (*F*) Arrows point to an example of a BrdUrd-incorporating cell in PBS-treated mice. Infrequent apoptotic bodies (arrows) visualized by TUNEL staining in tumor tissue from mock-treated (*G*) and toxin-treated (*J*) tumors demonstrate toxin-induced tumor cell killing in the absence of apoptosis-associated DNA fragmentation. (Bars = 10 μm.)

efficacy of the engineered toxin to T241 fibrosarcoma (28), B16-BL6 melanoma (27), and Lewis lung carcinoma (30). These three murine tumors are of widely different origin (connective tissue, neural crest, and pulmonary epithelium, respectively), are highly malignant, disseminate rapidly when transplanted to syngeneic mice, and demonstrate a poor response to conventional treatment. Mice bearing solid intradermal tumor nodules constituting ≈0.05–0.5% of the total body mass were treated either with PBS, one injection of 15 μg of PrAg-U2 with FP59, or two injections of the toxin at a 3-day interval (Fig. 3 *A–D*). All tumors were highly susceptible to the engineered toxin. A single treatment with PrAg-U2 and FP59 caused 92%, 85%, and 65% reductions in the sizes of fibrosarcoma, melanoma, and lung carcinoma, respectively, and two applications of the toxin caused 98%, 92%, and 86% reduction, respectively, of tumor size as compared with PBS-treated mice (Fig. 3 *A–C*). Furthermore, the tumors were completely eradicated in 67% of fibrosarcoma-bearing mice treated with just a single toxin injection, and in 88% of fibrosarcoma and 17% of melanoma-bearing mice treated with two applications of the toxin. Microscopic analysis of tumor tissue revealed tumor cell cytotoxicity already 12 h after toxin administration (data not shown). Tumor cell cytotoxicity was manifest at 24 h with gross cytoplasmic shrinkage, nuclear condensation, and complete cessation of BrdUrd incorporation (Fig. 3 *E*, *F*, *H*, and *I*). Moreover, tumor endothelial cell damage was profound, with tumor vessels displaying severe angiectasis, vascular stasis, and hemorrhaging (Fig. 3*H*). The engineered toxin did not cause an increase in tumor cell apoptosis, as assessed by TUNEL staining (Fig. 3 *G* and *J*), suggesting that toxin-treated tumor cells were predominantly undergoing necrotic cell death. Interestingly, the epidermis and hair follicles immediately adjacent to the tumors demonstrated no pathological changes, and continued cell proliferation was observed in basal keratinocytes of both the interfollicular epidermis and the hair follicles (Fig. 3 *H* and *I*). However, toxin treatment was associated with significant peritumoral edema and leukocyte infiltration. This reaction seemed to be triggered by extensive necrotic tumor cell death, because it was observed to only a minimal extent in non-tumor-bearing mice when injected intradermally with toxin (data not shown).

Tumor Cell-Surface Plg Activation Is Required for the Tumoricidal Activity of PrAg-U2. Plg is produced by the host and not by tumor cells (31) and is essential for the conversion of pro-uPA to two-chain uPA and the subsequent PrAg-U2 activation (see above). To determine the role of cell-surface uPA in tumor cell cytotoxicity of the engineered toxin, we therefore transplanted Lewis lung carcinoma to $Plg^{-/-}$ mice and Plg-sufficient control mice and treated the ensuing Plg-deprived and Plg-sufficient tumors with PrAg-U2 with FP59 (Fig. 4*A*). Tumors developed in all $Plg^{-/-}$ mice but were significantly smaller as compared with control mice (Fig. 4*A*), consistent with previous studies (31). Remarkably, however, the tumors growing in $Plg^{-/-}$ mice were completely unresponsive to treatment with the engineered toxin (Fig. 4*A*), demonstrating that Plg activation is absolutely required for PrAg-U2 activation and tumor cytotoxicity *in vivo*.

Tumor endothelial cells express both uPAR and tumor endothelium marker 8, suggesting that PrAg-U2 with FP59 may target tumor endothelium, and treatment of tumors with the engineered toxin did cause severe damage to tumor endothelial cells (Fig. 3*H*). To determine whether PrAg-U2 with FP59 displays direct cytotoxicity to tumor endothelium, Lewis lung carcinoma-bearing $uPAR^{-/-}$ mice (PrAg-U2-resistant stroma) and Lewis lung carcinoma-bearing wild-type control mice (PrAg-U2-sensitive stroma) were treated with PrAg-U2 with FP59 (Fig. 4*B*). Surprisingly, the engineered toxin killed tumors growing in $uPAR^{-/-}$ and uPAR-sufficient mice with equal efficacy (Fig. 4*B*), suggesting that the profound tumor endothe-

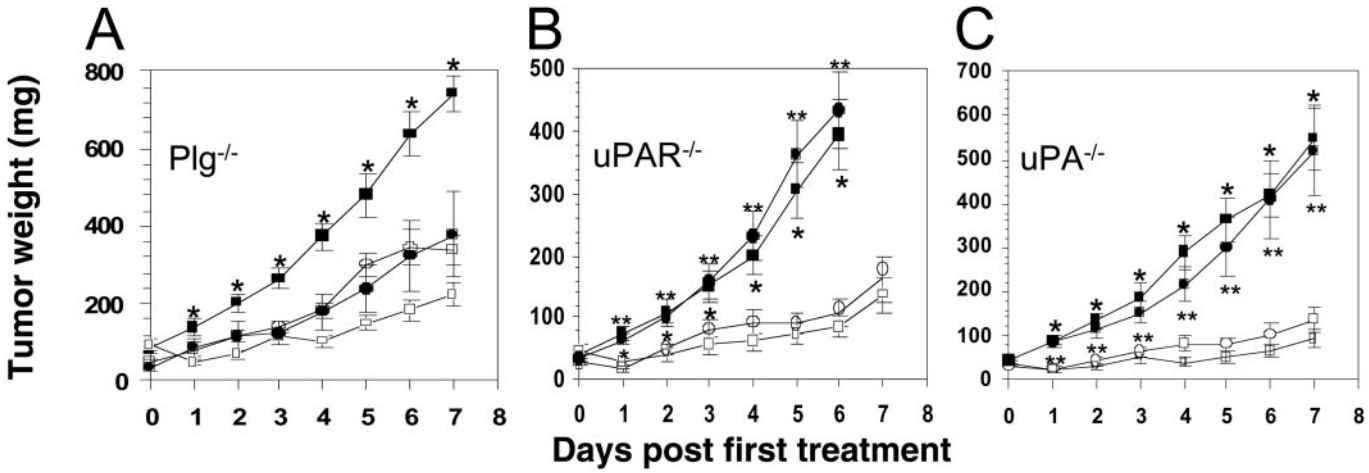

Fig. 4. Tumor cytotoxicity of PrAg-U2 depends on stromal Plg and tumor cell-derived uPAR and uPA. Lewis lung carcinoma-bearing $Plg^{-/-}$ (*A*), $uPAR^{-/-}$ (*B*), and $uPA^{-/-}$ (*C*) mice (circles) and congenic WT control mice (squares) were treated on day 0 and day 3 with PrAg-U2 with FP59 (○ and □) or PBS (● and ■). *, Significance ($P < 0.05$) of PBS treatment vs. PrAg-U2 treatment of WT mice; **, significance of PBS treatment vs. PrAg-U2 treatment of knockout mice.

lial cell damage caused by PrAg-U2 treatment is secondary to tumor cell cytotoxicity. We used a similar experimental rationale to determine whether the tumor cell-surface uPA that mediates the activation of PrAg-U2 was produced by the tumor cells (autocrine saturation of tumor cell uPAR) or by the tumor stromal cells (paracrine saturation of tumor cell uPAR). Lewis lung carcinoma-bearing $uPA^{-/-}$ mice and uPA-sufficient control mice were treated with PrAg-U2 with FP59, and the importance of stromal cell-produced uPA for PrAg-U2 activation was determined (Fig. 4*C*). The experiment revealed that PrAg-U2 impaired tumor growth with equal potency in the absence and presence of stromal uPA (Fig. 4*C*), demonstrating that autocrine saturation of tumor cell uPAR by tumor cell-produced uPA is sufficient for toxin activation and tumor cell killing in this tumor model.

Discussion

We took advantage of the vast expression of cell-surface uPA in tumors to design a cell-surface uPA-activated anthrax toxin with potent and broad therapeutic efficacy against malignant tumors. Notably, this engineered toxin efficiently suppressed malignant tumor growth and could eradicate established tumors in the absence of toxicity to normal tissue. The engineered toxin may have broad applicability for the treatment of human tumors because of its species-independent mode of activation and the copious expression of cell-surface uPA on human tumors, ranging from carcinoma and sarcoma to hematogenous malignancies. The presented design of a tumor cell cytotoxic anthrax toxin is extremely versatile and can be improved easily by additional modifications. These include refinements in the protease activation loop to provide increased protease specificity, the targeting of the toxin to other tumor- or tumor endothelial cell-surface proteases, changes of PrAg receptor specificity (32), and the use of other cytotoxic "passenger" proteins, such as the A subunit of *Shiga* toxin (33), LF (34, 35), or Bad (36). For example, human melanoma is extremely sensitive to LF, and recent work by Koo *et al*. (35) demonstrated that the combination of native PrAg with LF had therapeutic efficacy to xenografted human melanoma at a concentration that was tolerated by mice. LF might be delivered in higher concentrations to malignant melanoma by using PrAg-U2 rather than PrAg because of the highly attenuated toxicity of the uPA-activated version of PrAg. The strategy described here even can be adapted to greatly improve the therapeutic index of immunotoxins already in clinical use. For example, a diphtheria toxin/granulocyte macrophage colony-stimulating factor fusion protein has high efficacy against acute myeloid leukemia, but the pronounced hepatotoxicity limits the clinical applicability (37). Conferring uPA-dependent activation to the fusion toxin would be expected to eliminate this problem.

Its many virtues notwithstanding, therapeutic application of PrAg-U2 would be subject to the same general liabilities that are inherent to most antineoplastic drugs as well as to liabilities particular to the use of protein toxins. The latter would include the eventual development of prohibitive toxin-neutralizing antibodies and the poor penetration of the toxin into solid tumors. Moreover, many pharmacological parameters regarding tissue distribution and kinetics of the toxin will have to be studied to establish optimal routes of administration for the treatment of human malignancies.

The generation of an uPA-activated anthrax toxin thus provided an opportunity to test established paradigms regarding uPA-mediated cell-surface Plg activation *in vivo*. The pivotal role of uPAR in uPA-mediated cell-surface Plg activation is well defined biochemically (2), but the function of uPAR *in vivo* recently was challenged by the much milder phenotype of $uPAR^{-/-}$ mice compared with $uPA^{-/-}$ mice (8–10) and by the reports that certain cultured cells potentiate uPA-mediated Plg activation in the absence of uPAR (11). The data presented here unequivocally establish uPAR as critical for generating cell-surface uPA activity *in vivo*. Our data also show that plasmin is critical in the mouse for the conversion of pro-uPA to two-chain uPA, both in the context of physiological Plg activation and on the tumor cell surface. Other pro-uPA-activating proteases, such as Matriptase/MT-SP1, true tissue kallikrein, hepatocyte growth factor activator, and cathepsin B, if at all relevant, must serve more as initiators of the process of two-chain uPA generation (38–41). Finally, our data reveal that PAI-1 restricts the continuous generation of active cell-surface uPA *in vivo* in a number of tissues including the small intestine, primary and secondary lymphoid tissues, adrenal cortex, and osteoid.

LF is very stable in circulation when administered alone and becomes cell surface-associated only after the binding of PrAg to tumor endothelium marker 8 and its subsequent proteolytic cleavage to PrAg63 (13, 14). The technology presented here therefore also can be modified easily so as to achieve the *in vivo* imaging of cells expressing specific cell-surface proteolytic activity. LF residues 1–254 could be conjugated or fused to a number of detectable moieties including radionuclides, fluorochromes, enzymes such as β-lactamase, β-galactosidase, red and green fluorescent protein, or even magnetic resonance image

contrast agents to provide real-time, noninvasive imaging of specific cell-surface protease activity. PrAg and LF derivatives thus could be tailored to image any cell-surface protease for which a specific peptide substrate can be identified. Besides the obvious applications in basic research, such imaging agents may be clinically useful in the diagnostic profiling of human tumors and for monitoring the efficacy of specific protease inhibition *in vivo*.

In conclusion, we have demonstrated that changes in the proteolytic activation specificity can convert anthrax toxin to a potent antitumor agent with potentially broad therapeutic and diagnostic applicability.

We thank Drs. Henning Birkedal-Hansen, Silvio Gutkind, Alfredo Molinolo, Ulrike Lichti, and Mary Jo Danton for critically reading the manuscript and Dana Hsu for assistance with toxin purification.

1. Andreasen, P. A., Kjoller, L., Christensen, L. & Duffy, M. J. (1997) *Int. J. Cancer* **72,** 1–22.
2. Dano, K., Romer, J., Nielsen, B. S., Bjorn, S., Pyke, C., Rygaard, J. & Lund, L. R. (1999) *Acta Pathol. Microbiol. Immunol. Scand.* **107,** 120–127.
3. Andreasen, P. A., Egelund, R. & Petersen, H. H. (2000) *Cell Mol. Life Sci.* **57,** 25–40.
4. Romer, J., Bugge, T. H., Pyke, C., Lund, L. R., Flick, M. J., Degen, J. L. & Dano, K. (1996) *Nat. Med.* **2,** 287–292.
5. Lund, L. R., Bjorn, S. F., Sternlicht, M. D., Nielsen, B. S., Solberg, H., Usher, P. A., Osterby, R., Christensen, I. J., Stephens, R. W., Bugge, T. H., *et al.* (2000) *Development (Cambridge, U.K.)* **127,** 4481–4492.
6. Heymans, S., Luttun, A., Nuyens, D., Theilmeier, G., Creemers, E., Moons, L., Dyspersin, G. D., Cleutjens, J. P., Shipley, M., Angellilo, A., *et al.* (1999) *Nat. Med.* **5,** 1135–1142.
7. Nielsen, L. S., Hansen, J. G., Skriver, L., Wilson, E. L., Kaltoft, K., Zeuthen, J. & Dano, K. (1982) *Biochemistry* **21,** 6410–6415.
8. Bugge, T. H., Suh, T. T., Flick, M. J., Daugherty, C. C., Romer, J., Solberg, H., Ellis, V., Dano, K. & Degen, J. L. (1995) *J. Biol. Chem.* **270,** 16886–16894.
9. Bugge, T. H., Flick, M. J., Danton, M. J., Daugherty, C. C., Romer, J., Dano, K., Carmeliet, P., Collen, D. & Degen, J. L. (1996) *Proc. Natl. Acad. Sci. USA* **93,** 5899–5904.
10. Carmeliet, P., Moons, L., Dewerchin, M., Rosenberg, S., Herbert, J. M., Lupu, F. & Collen, D. (1998) *J. Cell Biol.* **140,** 233–245.
11. Longstaff, C., Merton, R. E., Fabregas, P. & Felez, J. (1999) *Blood* **93,** 3839–3846.
12. Smith, H. & Stanley, J. L. (1962) *J. Gen. Microbiol.* **29,** 517–521.
13. Leppla, S. H. (1995) in *Bacterial Toxins and Virulence Factors in Disease. Handbook of Natural Toxins*, eds. Moss, J., Iglewski, B., Vaughan, M. & Tu, A. (Dekker, New York), Vol. 8, pp. 543–572.
14. Leppla, S. H. (1999) in *Comprehensive Sourcebook of Bacterial Protein Toxins*, eds. Alouf, J. E. & Freer, J. H. (Academic, London), pp. 243–263.
15. Bradley, K. A., Mogridge, J., Mourez, M., Collier, R. J. & Young, J. A. (2001) *Nature* **414,** 225–229.
16. Molloy, S. S., Bresnahan, P. A., Leppla, S. H., Klimpel, K. R. & Thomas, G. (1992) *J. Biol. Chem.* **267,** 16396–16402.
17. Klimpel, K. R., Molloy, S. S., Thomas, G. & Leppla, S. H. (1992) *Proc. Natl. Acad. Sci. USA* **89,** 10277–10281.
18. Mogridge, J., Cunningham, K. & Collier, R. J. (2002) *Biochemistry* **41,** 1079–1082.
19. Arora, N. & Leppla, S. H. (1993) *J. Biol. Chem.* **268,** 3334–3341.
20. Liu, S., Netzel-Arnett, S., Birkedal-Hansen, H. & Leppla, S. H. (2000) *Cancer Res.* **60,** 6061–6067.
21. Carmeliet, P., Schoonjans, L., Kieckens, L., Ream, B., Degen, J., Bronson, R., De Vos, R., van den Oord, J. J., Collen, D. & Mulligan, R. C. (1994) *Nature* **368,** 419–424.
22. Bugge, T. H., Flick, M. J., Daugherty, C. C. & Degen, J. L. (1995) *Genes Dev.* **9,** 794–807.
23. Carmeliet, P., Kieckens, L., Schoonjans, L., Ream, B., van Nuffelen, A., Prendergast, G., Cole, M., Bronson, R., Collen, D. & Mulligan, R. C. (1993) *J. Clin. Invest.* **92,** 2746–2755.
24. Bugge, T. H., Kombrinck, K. W., Flick, M. J., Daugherty, C. C., Danton, M. J. & Degen, J. L. (1996) *Cell* **87,** 709–719.
25. Gordon, V. M., Benz, R., Fujii, K., Leppla, S. H. & Tweten, R. K. (1997) *Infect. Immunol.* **65,** 4130–4134.
26. Liu, S., Bugge, T. H. & Leppla, S. H. (2001) *J. Biol. Chem.* **276,** 17976–17984.
27. Hart, I. R. (1979) *Am. J. Pathol.* **97,** 587–600.
28. Liotta, L. A., Tryggvason, K., Garbisa, S., Hart, I., Foltz, C. M. & Shafie, S. (1980) *Nature* **284,** 67–68.
29. Geran, R. I., Greenberg, N. H., MacDonald, M. M., Schumacher, A. M. & Abbot, B. J. (1972) *Cancer Chemother. Rep.* **3,** 1–103.
30. Sugiura, K. & Stock, C. C. (1955) *Cancer Res.* **15,** 38–51.
31. Bugge, T. H., Kombrinck, K. W., Xiao, Q., Holmback, K., Daugherty, C. C., Witte, D. P. & Degen, J. L. (1997) *Blood* **90,** 4522–4531.
32. Varughese, M., Chi, A., Teixeira, A. V., Nicholls, P. J., Keith, J. M. & Leppla, S. H. (1998) *Mol. Med.* **4,** 87–95.
33. Arora, N. & Leppla, S. H. (1994) *Infect. Immunol.* **62,** 4955–4961.
34. Duesbery, N. S., Resau, J., Webb, C. P., Koochekpour, S., Koo, H. M., Leppla, S. H. & Vande Woude, G. F. (2001) *Proc. Natl. Acad. Sci. USA* **98,** 4089–4094.
35. Koo, H. M., VanBrocklin, M., McWilliams, M. J., Leppla, S. H., Duesbery, N. S. & Vande Woude, G. F. (2002) *Proc. Natl. Acad. Sci. USA* **99,** 3052–3057.
36. Ichinose, M., Liu, X. H., Hagihara, N. & Youle, R. J. (2002) *Cancer Res.* **62,** 1433–1438.
37. Frankel, A. E., Powell, B. L., Hall, P. D., Case, L. D. & Kreitman, R. J. (2002) *Clin. Cancer Res.* **8,** 1004–1013.
38. Lee, S. L., Dickson, R. B. & Lin, C. Y. (2000) *J. Biol. Chem.* **275,** 36720–36725.
39. List, K., Jensen, O. N., Bugge, T. H., Lund, L. R., Ploug, M., Dano, K. & Behrendt, N. (2000) *Biochemistry* **39,** 508–515.
40. Romisch, J., Vermohlen, S., Feussner, A. & Stohr, H. (1999) *Haemostasis* **29,** 292–299.
41. Takeuchi, T., Harris, J. L., Huang, W., Yan, K. W., Coughlin, S. R. & Craik, C. S. (2000) *J. Biol. Chem.* **275,** 26333–26342.